© Pol J Radiol 2023; 88: e203-e215
DOI: https://doi.org/10.5114/pjr.2023.127058

Received: 24.11.2022
Accepted: 15.01.2023
Published: 14.04.2023

Polish Journal of Radiology

http://www.polradiol.com

Original paper

Differentiation of various salivary gland tumours using diffusion-weighted MRI and dynamic contrast-enhanced MRI

Mohini Kushwaha[1,B,C,D,E,F], Jyoti Kumar[1,A,B,D,E,F], Anju Garg[1,B,D,E,F], Ishwar Singh[2,B,D], Nita Khurana[3,B,D]

[1]Department of Radiodiagnosis, Maulana Azad Medical College, New Delhi, Delhi, India
[2]Department of Otorhinolaryngology, Head and Neck Surgery, Maulana Azad Medical College, New Delhi, Delhi, India
[3]Department of Pathology, Maulana Azad Medical College, New Delhi, Delhi, India

Abstract

Purpose: To determine the role of functional magnetic resonance imaging techniques (diffusion-weighted magnetic resonance imaging [DW-MRI] and dynamic contrast-enhanced magnetic resonance imaging [DCE-MRI]) in the differentiation of various salivary gland tumours.

Material and methods: In this prospective study, we evaluated 32 patients with salivary gland tumours using functional MRI. Diffusion parameters (mean apparent diffusion coefficient [ADC], normalized ADC and homogeneity index [HI]), semiquantitative DCE parameters (time signal intensity curves [TICs]) and quantitative DCE parameters (K_{ep}, K_{trans} and V_e) were analysed. Diagnostic efficiencies of all these parameters were determined to differentiate benign and malignant tumours as well as to characterize 3 major subgroups of salivary gland tumours, namely pleomorphic adenoma, Warthin tumour, and malignant tumours.

Results: Mean ADC, normalized ADC and HI were insignificant in differentiating benign and malignant tumours but were significant in differentiating pleomorphic adenomas, Warthin tumours, and malignant tumours. Mean ADC was the best parameter in predicting both pleomorphic adenomas and Warthin tumours (AUC: 0.95 and 0.89, respectively). Amongst DCE parameters, only TIC pattern could differentiate between benign and malignant tumours, with an accuracy of 93.75% (AUC: 0.94). The quantitative perfusion parameters aided greatly in characterizing pleomorphic adenomas, Warthin tumours and malignant tumours. For predicting pleomorphic adenomas, the accuracy of K_{ep} and K_{trans} was 96.77% (AUC: 0.98) and 93.55% (AUC: 0.95), respectively and for predicting Warthin tumours, the accuracy of both K_{ep} and K_{trans} was 96.77% (AUC: 0.97).

Conclusions: DCE parameters (particularly TIC, K_{ep} and K_{trans}) had higher accuracy in characterizing various tumour subgroups (pleomorphic adenomas, Warthin tumours, and malignant tumours) than DWI parameters. Hence, dynamic contrast-enhanced imaging adds immense value with only a minimum time penalty to the examination.

Key words: diffusion, salivary gland tumours, dynamic contrast-enhanced imaging.

Introduction

Salivary gland tumours account for only 3% of all head and neck tumours but encompass a wide variety of histopathologically distinct entities [1]. Clinical findings alone are often insufficient in differentiating benign tumours from malignant ones because the most common clinical presentation is that of a painless palpable mass in both cases. There is marked pathological heterogeneity within each of these subgroups. The prognosis and management of these tumours are significantly different. The sensitivity of pre-operative FNAC in differentiating benign and malignant salivary gland tumours is variable in different studies (52.0-98.5%) [2-5]. In addition, FNAC is especially difficult for tumours involving the deep lobe of the parotid gland.

Correspondence address:
Prof. Jyoti Kumar, Maulana Azad Medical College, Bahadurshah Zafar Marg, 110002, New Delhi, Delhi, India, e-mail: drjyotikumar@gmail.com

Authors' contribution:
A Study design · **B** Data collection · **C** Statistical analysis · **D** Data interpretation · **E** Manuscript preparation · **F** Literature search · **G** Funds collection

Therefore, pre-operative imaging of the salivary gland tumours is imperative not only to map the extent of the lesion but also to characterize the tumour.

Magnetic resonance imaging (MRI), because of its higher soft tissue resolution, is more effective than CT in the evaluation of salivary gland tumours. It is particularly helpful in evaluating extraglandular invasion, perineural spread and extra-capsular invasion in the case of nodal metastases [6].

Functional MR imaging techniques such as diffusion-weighted magnetic resonance imaging (DW-MRI) and dynamic contrast-enhanced magnetic resonance imaging (DCE-MRI) may play a role in predicting tumour histology. Diffusion-weighted imaging (DWI) has been used as an adjunct to conventional MRI sequences in nearly all body systems to provide valuable information regarding tumour cellularity and internal characteristics (such as necrotic and cystic degeneration). More recently, dynamic contrast-enhanced (DCE) imaging is being investigated as a tool for non-invasive assessment of perfusion and capillary permeability of tumours.

This study aims to evaluate salivary gland tumours using morphological as well as functional MR imaging techniques and compare the findings with pathological diagnosis.

Material and methods

Between October 2019 and October 2021, 32 consecutive patients ≥ 12 years old with a provisional diagnosis of salivary gland tumour detected either on clinical examination or on previous CT were included in this study. Patients with previous history of treatment for salivary gland tumour (post-operative/post-chemoradiotherapy) and patients with contra-indication to MRI/MR contrast were excluded from the study. Approval of the institutional Ethics Committee (F.1/IEC/MAMC/ [70/05/2019/No 566]) was obtained for the study and written informed consent was acquired from all patients.

Imaging technique

All patients underwent MR examination (including DWI and DCE-MRI) of the face and neck region in a supine position on a 3T MR system (MAGNETOM SKYRA; Siemens, Erlangen, Germany) using a dedicated 32-channel phased-array head coil.

A standardized imaging protocol was followed for all patients and the pulse sequences that were used are summarized in Table 1.

- **Diffusion-weighted image** acquisition was followed by generation of apparent diffusion coefficient (ADC) maps.
- Prior to **dynamic image acquisition**, pre-contrast T1 mapping was obtained with 2 flip angles of 2° and 10°, after which DCE- MRI was performed. 0.1 mmol/kg body weight of intravenous meglumine gadoterate (VividScan, Vivere Imaging, India) was injected after the 5th dynamic sequence at a rate of 2 ml/sec, followed by a 20-ml saline flush. In total, 50 dynamic sequences were performed every 5.03 seconds with 20 slices in each sequence (first 5 dynamic sequences of pre-contrast and 45 sequences of post-contrast images). The total duration of the dynamic scan was 4.17 minutes.
- This was followed by post-contrast T1-weighted fat-saturated images.

Image analysis

All the parameters were assessed independently by 2 head and neck radiologists with 16 and 23 years of experience, respectively. They were also blinded to the pathology results. The difference in opinion was resolved by consensus.

Morphological analysis

The MR images were assessed for the following morphological parameters: localization of the tumour (parotid [superficial lobe/deep lobe/both], submandibular or minor salivary gland), shape (round, oval, lobulated, irregular), margins (well-defined/ill-defined), and aspect (homogeneous/inhomogeneous).

The signal was characterized as iso-/hypo-/hyperintense relative to that of muscle on T1W and contralateral salivary gland on T2W images. When the signal intensity (SI) of the tumour was close to that of water on T2W images, it was assigned as markedly hyperintense.

Internal characteristics (cystic spaces/necrosis/haemorrhage/septations), enhancement pattern (homogeneous/heterogeneous/peripheral) of the tumour, extraglandular extension and infiltration into surrounding muscles, subcutaneous tissues and skin, bone changes, cervical lymphadenopathy and perineural spread were also assessed.

Diffusion-weighted MRI analysis

ADC values were obtained by placing 3 ROIs (regions of interest), each of at least 0.1 cm^2 over the solid component of the lesion on ADC maps generated from DW-MRI, avoiding the cystic/necrotic/haemorrhagic components, and the mean ADC was calculated.

Normalized ADC was calculated using the following formula [7]:

$$ADC_{Normalized} = \frac{(ADC_{lesion} - ADC_{C/L\ normal\ gland}) \times 100\%}{ADC_{C/L\ normal\ gland}}$$

where ADC_{lesion} was the mean ADC of the lesion and $ADC_{C/L\ normal\ gland}$ was the ADC value of the contralateral normal gland.

Homogeneity index (HI) was calculated using the following formula [8]:

$$\text{Homogeneity index} = \frac{ADC_{SD}}{\text{mean ADC}}$$

where ADC_{SD} was the standard deviation (SD) of the ADC.

Table 1. Imaging protocol and pulse sequences for MRI examination

Sequence		Plane	TR (ms)	TE (ms)	Intersection gap (mm)	Slice thickness (mm)	Matrix
STIR		Coronal	3200-3870	47-48	1-2	3	256 × 256
T1-weighted spin-echo images		Axial and coronal	550-811	9.4 -11	1-2	3	256 × 256
T2-weighted turbo spin-echo images		Axial and coronal	4800-7610	75-103	1-2	3	256 × 256
Readout segmentation of long variable echo trains (RESOLVE) DWI	*b*-values: 50 and 1000 s/mm^2	Axial	4270-6840	58-65	1-2	3.5	256 × 256
Time-resolved angiography with interleaved stochastic trajectories (TWIST) DCE-MRI	Flip angle: 12°	Axial	4.91	1.9	1-2	3.5	256 × 256
Post-contrast fat-saturated T1-weighted images		Axial and coronal	585-1110	10-11	1-2	3 mm	256 × 256

MRI – magnetic resonance imaging, DWI – diffusion-weighted imaging, DCE – dynamic contrast-enhanced, TR – repetition time, TE – echo time, STIR – short-T1 inversion recovery

Dynamic contrast-enhanced MRI analysis

Semiquantitative analysis: DCE-MRI was based on time signal intensity curves (TICs). These were obtained by placing an ellipse ROI of at least 0.1 cm^2 over the enhancing solid component of the lesion and avoiding the cystic, necrotic, haemorrhagic components/blood vessels. Time to peak (TTP) and washout ratios (WR) were derived from TICs.

The TICs obtained were categorized into 4 types (Figure 1) based on TTP and WR as described by Yabuuchi *et al.* [9].

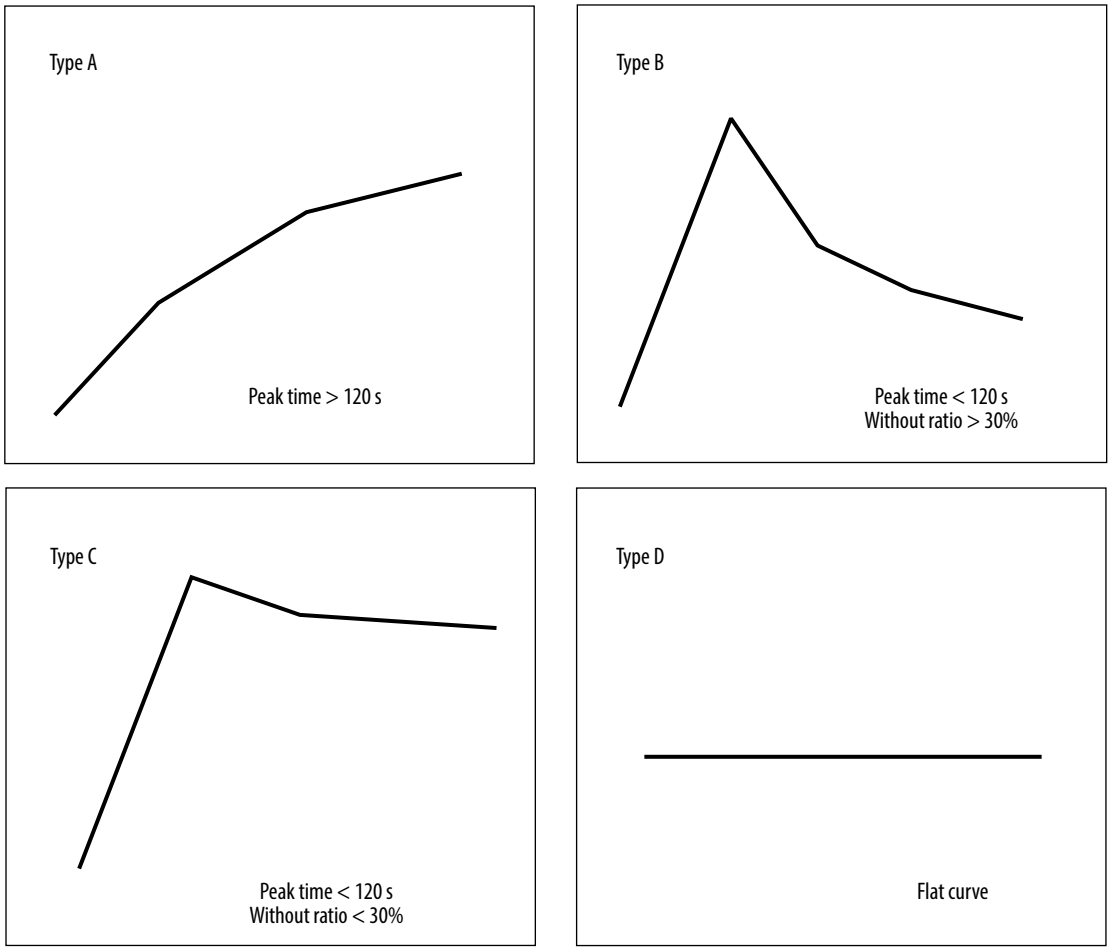

Figure 1. Types of time intensity curves (TICs) (according to Yabuuchi *et al.* [9])

Quantitative analysis: Quantitative assessment of DCE images was performed using the Toft model. Quantitative parameters K_{ep}, K_{trans} and V_e were obtained by placing an ellipse ROI of at least 0.1 cm^2 over the enhancing solid component of the lesion in the perfusion maps.

A provisional radiological diagnosis was made in 32 patients of salivary gland tumours, which was then compared with the cytological/histopathological diagnosis (gold standard). Histopathological diagnosis was available for 26 cases. For the remaining 6 cases, all Warthin tumours, cytological findings were taken as the gold standard because these were managed conservatively. Morphological characteristics, diffusion characteristics, and DCE imaging characteristics were compared between benign and malignant subgroups of salivary gland tumours. Since pleomorphic adenoma and Warthin tumours formed the bulk of benign salivary gland tumours, both with different imaging characteristics, prognoses, and management strategies, comparison of MR imaging characteristics was also done between pleomorphic adenomas, Warthin tumours, and malignant subgroups of tumours.

Statistical analysis

The collected data were transformed into variables, coded and entered in Microsoft Excel. The data were analysed and statistically evaluated using SPSS-PC-25. Quantitative data are expressed as mean ± standard deviation or median with interquartile range, and differences between 2 comparable groups were tested by Student's *t*-test (unpaired) or Mann-Whitney *U* test, while for comparison between more than 2 groups, the ANNOVA test or Kruskal-Wallis *H* test was used. Qualitative data were expressed in percentages, and the statistical differences between the proportions were tested using the chi-square test or Fisher exact test. The cut-off values for various DWI and DCE parameters were determined by receiver operating characteristic (ROC) curves, and the sensitivity, specificity, positive predictive value (PPV), negative predictive value (NPV) and diagnostic accuracy were calculated. A *p*-value of less than 0.05 was considered statistically significant.

Results

Demographic and histopathological results

A total of 32 patients were included in the study (18 males and 14 females) with ages ranging from 12 years to 76 years.

Facial swelling was the most common presenting symptom (90.6%) followed by oral cavity swelling (9.3%) seen in cases of minor salivary gland tumours. Signs of facial nerve palsy and rapid growth of swelling were observed in one case of carcinoma ex-pleomorphic adenoma.

The parotid gland was the most commonly involved salivary gland (n = 27, 84.37%), followed by minor salivary glands (n = 3, 9.37%) and submandibular gland (n = 2, 6.25%).

Sixteen (50%) of the patients had benign and 16 (50%) had malignant tumours. The final pathological diagnosis was as follows: pleomorphic adenoma (n = 8), Warthin tumour (n = 7), plexiform neurofibroma (n = 1), mucoepidermoid carcinoma (n = 8), carcinoma ex-pleomorphic adenoma (n = 3), adenoid cystic carcinoma (n = 1), secretory carcinoma (n = 1), non-Hodgkin B-cell lymphoma (n = 1), epithelial-myoepithelial carcinoma (n = 1) and parotid metastasis from carcinoma of an unknown primary (n = 1).

Bilateral and multifocal involvement was seen in 2 cases of Warthin tumours. In both the cases, imaging characteristics were evaluated for the dominant lesion.

Morphological characteristics

Amongst all the morphological characteristics that were assessed, irregular shape (p = 0.01), ill-defined margins (p <0.01) and infiltration into muscle, skin, and subcutaneous tissue (p = 0.03) were the only features that favoured malignancy and could significantly differentiate benign and malignant salivary gland tumours (Table 2). Markedly hyperintense SI on T2WI was only found in 5 benign tumours, all of which were pleomorphic adenomas (n = 8). Hence, markedly hyperintense SI approaching that of fluid strongly favoured the diagnosis of pleomorphic adenoma.

DW-MRI

Benign versus malignant tumours

The mean ADC value of benign tumours was 1.26 ± 0.53 × 10^{-3} mm^2/s and that of malignant tumours was 1.04 ± 0.21 × 10^{-3} mm^2/s. It was statistically insignificant in differentiating benign and malignant tumours (p = 0.35). Similar to the mean ADC value, the mean normalized ADC value (p = 0.54) and mean HI (p = 0.65) were statistically insignificant in differentiating benign and malignant tumours due to considerable overlap between the 2 groups.

Pleomorphic adenomas versus Warthin tumours versus malignant tumours

Table 3 shows the mean ADC values, mean normalized ADC values and mean homogeneity index of the 3 groups (pleomorphic adenoma, Warthin tumour and malignant tumour) and these were significant in differentiating pleomorphic adenomas, Warthin tumours and malignant tumours. The mean ADC and mean normalized ADC of pleomorphic adenoma were the highest, followed by those of malignant tumours. These were the least for

Table 2. Morphological characteristics of salivary gland tumours

Imaging features		Benign ($n = 16$)		Malignant ($n = 16$)		p-value
		n	%	n	%	
Shape	Round	5	31.25	1	6.25	0.17
	Oval	3	18.75	4	25	1
	Lobulated	7	43.75	3	18.75	0.25
	Irregular	1	6.25	8	50	0.01
Margins	Well-defined	15	93.75	3	18.75	< 0.01
	Ill-defined	1	6.25	13	81.25	
Aspect	Homogeneous	6	37.50	1	6.25	0.08
	Inhomogeneous	10	62.50	15	93.75	0.08
Predominant T1 signal	Hypointense	4	25	3	18.75	1
	Isointense	8	50	11	68.75	0.47
	Hyperintense	4	25	2	12.5	0.65
Predominant T2 signal	Hypointense	8	50	8	50	1
	Isointense	2	12.50	6	37.50	0.22
	Hyperintense	1	6.25	2	12.50	1
	Markedly hyperintense	5	31.25	0	0	0.04
Internal characteristics	Cystic spaces	3	18.75	5	31.25	0.68
	Haemorrhage	1	6.25	2	12.50	1
	Necrosis	3	18.75	6	37.50	0.43
	Septations	2	12.50	1	6.25	1
Enhancement	Homogeneous	4	25	2	12.50	0.65
	Heterogeneous	11	68.75	13	81.25	0.68
	Peripheral	1	6.25	1	6.25	1
Infiltration of muscle, skin, and subcutaneous tissue		1	6.25	7	43.75	0.03
Bone changes		1	6.25	3	18.75	0.59
Perineural invasion		0	0	2	12.50	0.10
Lymphadenopathy		2	12.50	5	31.25	0.39

Table 3. Comparison of DWI parameters in pleomorphic adenomas, Warthin tumours, and malignant tumours

Type of tumour	Mean ADC	Mean normalised ADC	Homogeneity index
Pleomorphic adenoma	1.65 ± 0.42	110.73 ± 80.89	0.06 ± 0.02
Warthin tumour	0.78 ± 0.16	–5.92 ± 26.51	0.11 ± 0.02
Malignant tumour	1.04 ± 0.21	24.58 ± 28.84	0.09 ± 0.03
***p*-value**	**< 0.001**	**< 0.001**	**< 0.001**

DWI – diffusion-weighted imaging, ADC – apparent diffusion coefficient

Warthin tumours. Unlike the mean ADC and normalized ADC, HI was the highest for Warthin tumours and lowest for pleomorphic adenomas.

Using ROC curve analysis (Figures 2 and 3), cut-off values and sensitivity, specificity, accuracy, PPV, and NPV of mean ADC, normalized ADC and HI were determined for predicting pleomorphic adenomas and Warthin tumours, as summarized in Tables 5 and 6, respectively. Amongst DWI parameters, mean ADC showed the maximum area under the curve (AUC) for predicting pleomorphic adenomas (AUC: 0.95) as well as Warthin tumours (AUC: 0.89).

DCE-MRI

TIC pattern

The type of TIC pattern could not only differentiate benign and malignant tumours ($p < 0.001$) but could also differen-

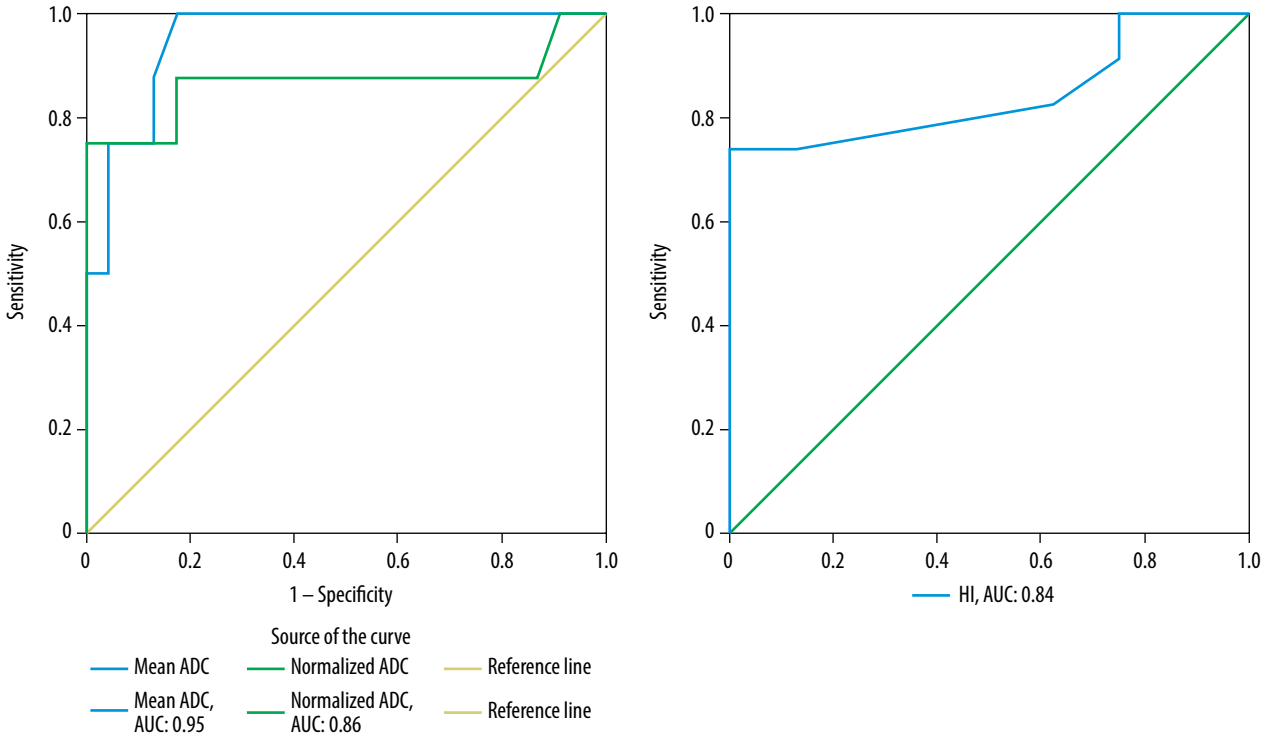

Figure 2. ROC curve analysis of DWI parameters: **A)** mean ADC, normalized ADC, and **B)** homogeneity index for the prediction of pleomorphic adenoma

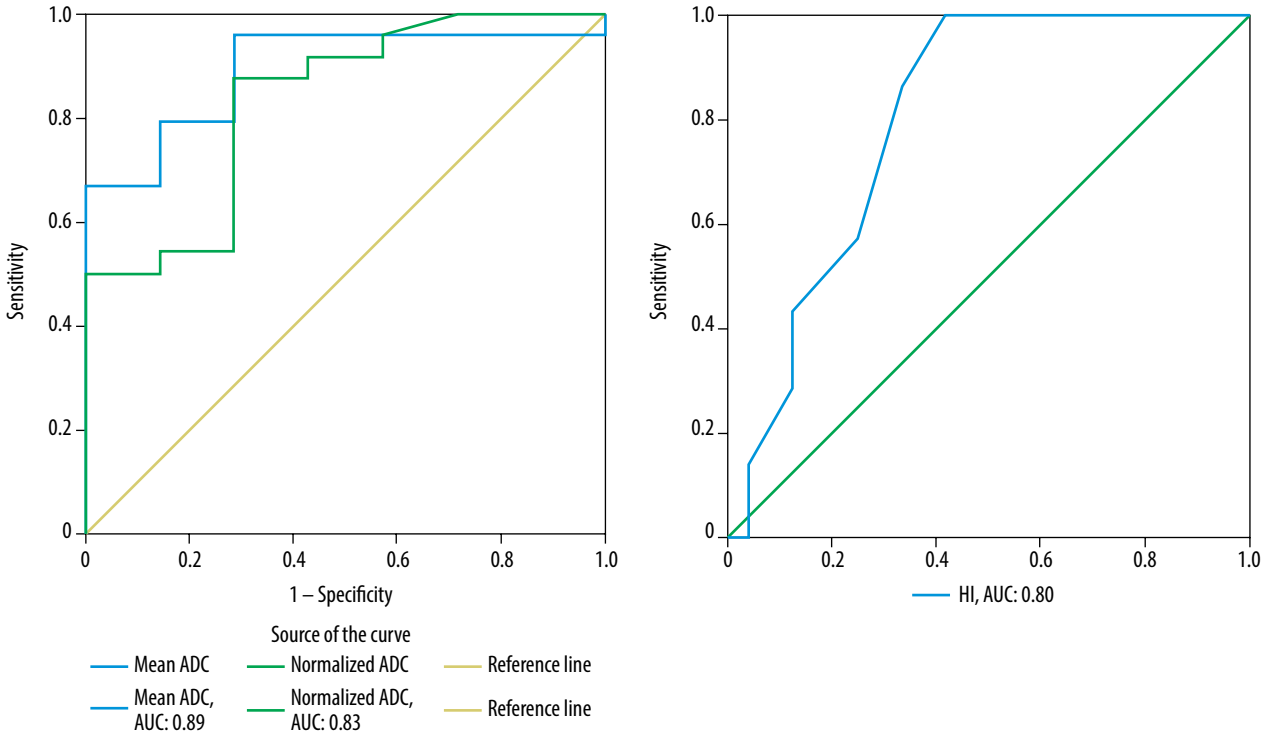

Figure 3. ROC curve analysis of DWI parameters (mean ADC, normalized ADC, and homogeneity index) for the prediction of Warthin tumours

tiate pleomorphic adenomas, Warthin tumours and malignant tumours from each other. All pleomorphic adenomas demonstrated type A TIC pattern while Warthin tumours demonstrated type B TIC curve (one case of Warthin tumour could not be evaluated on TIC due to its predominantly cystic morphology). 87.5% of cases of malignant tumours displayed type C TIC pattern (Figure 4).

TIC pattern was the only parameter that was found to be significant in differentiating benign and malignant salivary gland tumours. Using ROC curve analysis of TIC (Figure 5), type C TIC curve could detect malignant tumours with a sensitivity of 87.5%, specificity of 100%, PPV of 100%, NPV of 88.9% and accuracy of 93.75% (AUC of 0.94).

Table 4. Comparison of quantitative DCE-MRI parameters in pleomorphic adenomas, Warthin tumours and malignant tumours

Type of tumour	Mean K_{ep}	Mean K_{trans}	Mean V_e
Pleomorphic adenoma	0.17 ± 0.09	0.07 ± 0.04	0.46 ± 0.28
Warthin tumour	3.59 ± 1.85	0.61 ± 0.33	0.17 ± 0.04
Malignant tumour	0.86 ± 0.54	0.20 ± 0.13	0.25 ± 0.10
***p*-value**	**< 0.001**	**< 0.001**	**< 0.01**

DCE-MRI – dynamic contrast-enhanced magnetic resonance imaging, K_{ep} – rate constant from EES to plasma, V_e – extravascular extracellular space fractional volume

Table 5. Diagnostic performance of DWI and DCE-MRI parameters in diagnosing pleomorphic adenomas

MRI sequences	Parameters		Cut off values	Sensitivity (%)	Specificity (%)	PPV (%)	NPV (%)	Accuracy (%)
DCE-MRI	TIC pattern		Type A	100	91.30	80	100	93.55
	Quantitative DCE-MRI parameters	K_{ep}	0.36 min^{-1}	100	95.65	88.89	100	96.77
		K_{trans}	0.089 min^{-1}	75	100	100	92	93.55
		V_e	0.289	87.50	86.96	70	95.24	87.1
DWI	Mean ADC value		1.14×10^{-3} mm^2/s	100	82.6	66.67	100	87.1
	$ADC_{normalized}$		78%	75	100	100	92	93.55
	HI		0.089	100	73.91	57.14	100	80.65

MRI – magnetic resonance imaging, DWI – diffusion-weighted imaging, DCE-MRI – dynamic contrast-enhanced magnetic resonance imaging, TIC – time intensity curve, K_{trans} – volume transfer constant from blood plasma to EES, K_{ep} – rate constant from EES to plasma, V_e – extravascular extracellular space fractional volume, ADC – apparent diffusion coefficient, HI – homogeneity index, PPV – positive predictive value, NPV – negative predictive value

Table 6. Diagnostic performance of DWI and DCE-MRI parameters in diagnosing Warthin tumours

MRI sequences	Parameters		Cut-off values	Sensitivity (%)	Specificity (%)	PPV (%)	NPV (%)	Accuracy (%)
DCE-MRI	TIC pattern		Type B	100	96	85.71	100	96.77
	Quantitative DCE-MRI parameters	K_{ep}	1.34 min^{-1}	100	95.70	88.89	100	96.77
		K_{trans}	0.288 min^{-1}	100	95.70	88.89	100	96.77
		V_e	0.181	66.70	87.50	57.14	91.33	83.33
DWI-MRI	Mean ADC value		0.82×10^{-3} mm^2/s	71.40	95.80	83.33	92	90.32
	$ADC_{normalized}$		–0.88%	71.40	87.50	62.50	91.30	83.87
	HI		0.09	100	58.30	41.20	100	67.74

MRI – magnetic resonance imaging, DWI – diffusion-weighted imaging, DCE-MRI – dynamic contrast-enhanced magnetic resonance imaging, TIC – time intensity curve, K_{trans} – volume transfer constant from blood plasma to EES, K_{ep} – rate constant from EES to plasma, V_e – extravascular extracellular space fractional volume, ADC – apparent diffusion coefficient, HI – homogeneity index, PPV – positive predictive value, NPV – negative predictive value

Using type A TIC pattern, pleomorphic adenoma could be diagnosed and using type B TIC pattern, Warthin tumour could be diagnosed, with high sensitivity, specificity, and accuracy (Tables 5 and 6).

Quantitative DCE parameters

Benign versus malignant tumours

The mean K_{ep} of benign and malignant tumours was 1.545 min^{-1} and 0.861 min^{-1}, respectively. The mean K_{trans} of benign and malignant tumours was 0.286 min^{-1} and 0.200 min^{-1}, respectively. The mean V_e of benign and malignant tumours was 0.316 and 0.250, respectively. These were statistically insignificant (K_{ep}: $p = 0.32$; K_{trans}: $p = 0.42$; and V_e: $p = 0.78$) in differentiating benign from malignant tumours.

Pleomorphic adenomas versus Warthin tumours versus malignant tumours

Table 4 shows the mean quantitative DCE parameters (K_{ep}, K_{trans} and V_e) of pleomorphic adenoma, Warthin tumours and malignant tumours, which were significant in differentiating pleomorphic adenoma, Warthin tumours and malignant tumours from each other. While pleomorphic adenomas had the lowest mean K_{ep} and K_{trans} and the highest V_e, Warthin tumours had the highest mean K_{ep} and K_{trans} and the lowest V_e among the 3 groups.

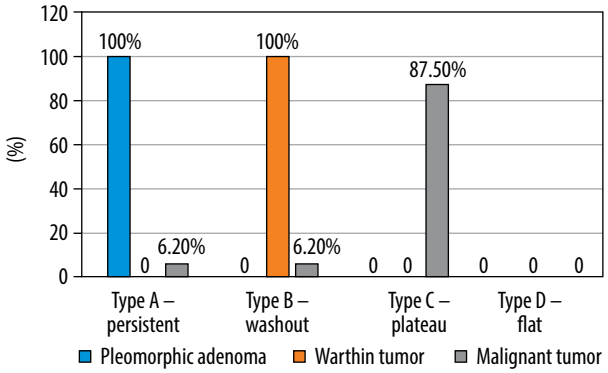

Figure 4. Comparison of time intensity curve (TIC) pattern of pleomorphic adenomas, Warthin tumours, and malignant tumours

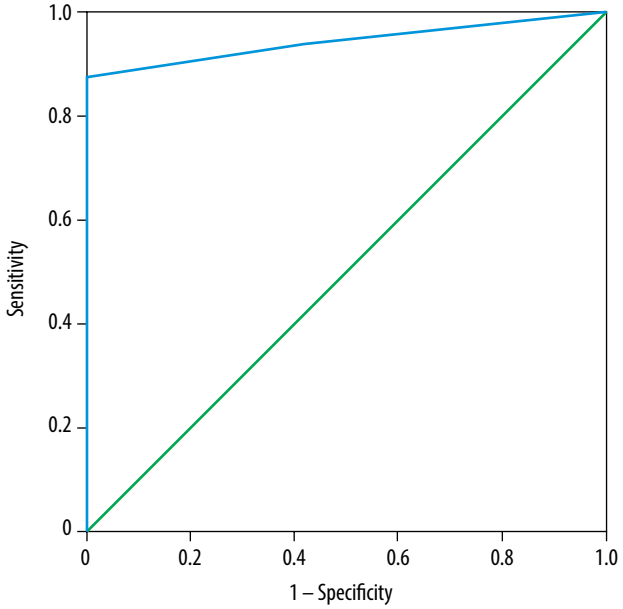

Figure 5. ROC curve analysis of time intensity curve (TIC) pattern for differentiation between benign and malignant salivary gland tumours

ROC curve analysis (Figures 6 and 7) for predicting pleomorphic adenoma and Warthin tumours revealed cut-off values, sensitivity, specificity, PPV, NPV, and diagnostic accuracy as demonstrated in Tables 5 and 6, respectively.

Diagnostic efficiency of various DWI and DCE parameters in differentiating various salivary gland tumours

Tables 5 and 6 show cut-off values and diagnostic efficiency of various DWI and DCE parameters in diagnosing pleomorphic adenomas and Warthin tumours.

K_{ep} was the best parameter in distinguishing pleomorphic adenoma from others, with an accuracy of 96.77% and AUC of 0.98. Following K_{ep}, TIC pattern (type A), K_{trans} and normalized ADC achieved comparable accuracy (93.55%). TIC pattern (type B), K_{ep} and K_{trans} achieved high and comparable accuracy (96.77%, AUC: 0.97) for diagnosing Warthin tumours and distinguishing them from pleomorphic adenomas and malignant tumours.

Discussion

Benign versus malignant tumours

TIC pattern was the only parameter that could distinguish benign and malignant tumours. Type A and type B curves were displayed by 100% of pleomorphic adenomas and Warthin tumours, respectively, reflecting benign aetiology. On the other hand, a type C curve was shown by the majority of the malignant tumours, achieving high sensitivity (87.5%), specificity (100%) and accuracy (93.75%) in differentiating malignant tumours from benign ones. The results were consistent with previous studies, all of which demonstrated that type A and type B curve are seen in benign tumours and type C curve in malignant tumours [9-12].Only 2 malignant tumours (one adenoid cystic carcinoma and another epithelial myoepithelial carcinoma) did not show type C TIC pattern. Adenoid cystic carcinoma demonstrated a type A curve, probably due to abundant myxoid component [13]. Type B TIC (high WR) in one case of epithelial myoepithelial carcinoma could point towards its highly cellular nature.

None of the DWI and DCE quantitative parameters (mean ADC, normalized ADC, HI, K_{ep}, K_{trans} and V_e) were significant in differentiating benign and malignant tumours due to considerable overlap. Other studies have found varied results. Most studies have found no significant differences between ADC of benign and malignant tumours [14-17]. However, Karaman *et al.* [18] and Karaman *et al.* [19] determined a cut-off value of 1.4×10^{-3} mm^2/s and 1.2×10^{-3} mm^2/s to differentiate benign from malignant tumours, respectively. This may be attributed to a high proportion of lymphoma patients (comprising of 44.4% of the malignant cases in the former and 33.3% in the latter) in both these studies, thus lowering mean ADC of malignant tumours and significantly differentiating it from benign tumours.

Another study by Zhang *et al.* [7] found significant differences between normalized ADC of benign (20.8 ± 40.9%) and malignant tumours (–13.2 ± 34.8%) and determined a cuff-off value of –0.45% to differentiate the 2 groups. However, the study had a low sensitivity and specificity of 65% and 70%, respectively.

Pleomorphic adenomas versus Warthin tumours versus malignant tumours

Diffusion-weighted imaging

Mean ADC values were found to be statistically significant in differentiating pleomorphic adenomas, Warthin tumours and malignant tumours from each other ($p < 0.001$). ADC $> 1.14 \times 10^{-3}$ mm^2/s strongly favoured pleomorphic adenomas and $< 0.82 \times 10^{-3}$ mm^2/s favoured Warthin tumours. Similar results were shown by Yabuuchi *et al.* [20], who determined a cut-off of 1.4×10^{-3} mm^2/sec between pleomorphic adenomas and malignant tumours and 1×10^{-3} mm^2/sec between Warthin tumours and malignant tumours.

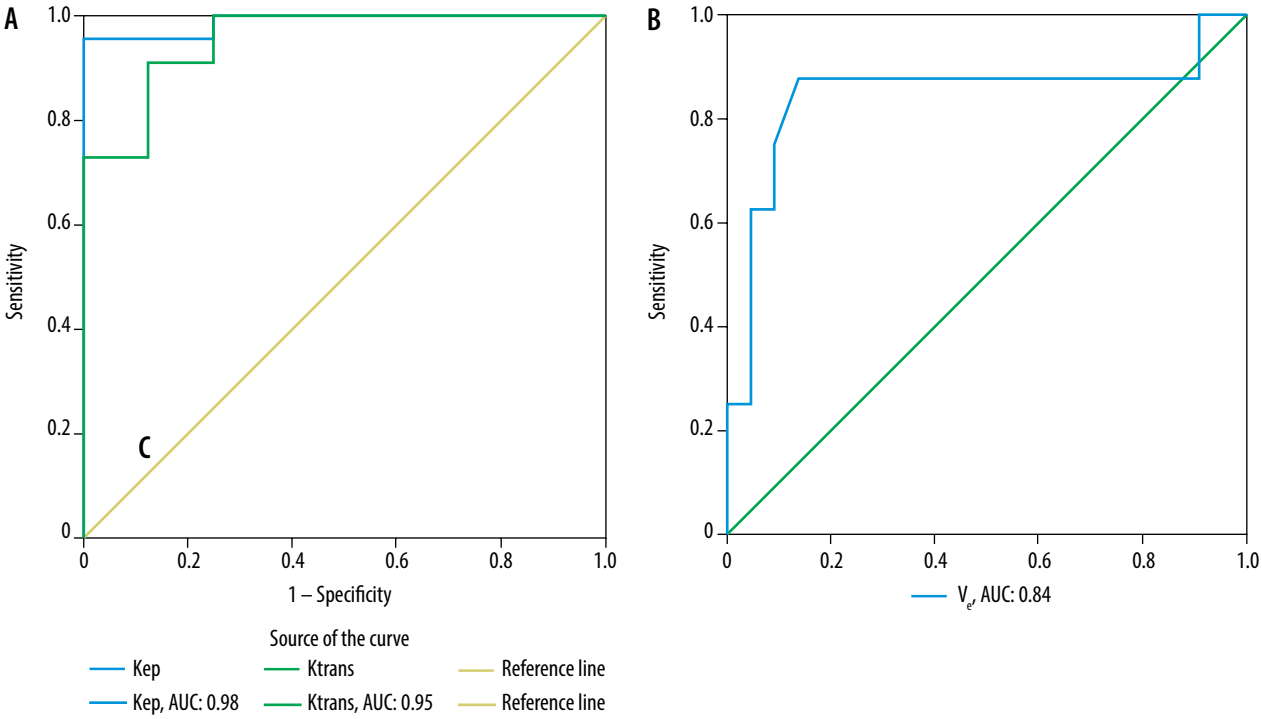

Figure 6. ROC curve analysis of quantitative DCE-MRI parameters (K_{ep}, K_{trans} – **A**, and V_e – **B**) for the prediction of pleomorphic adenomas

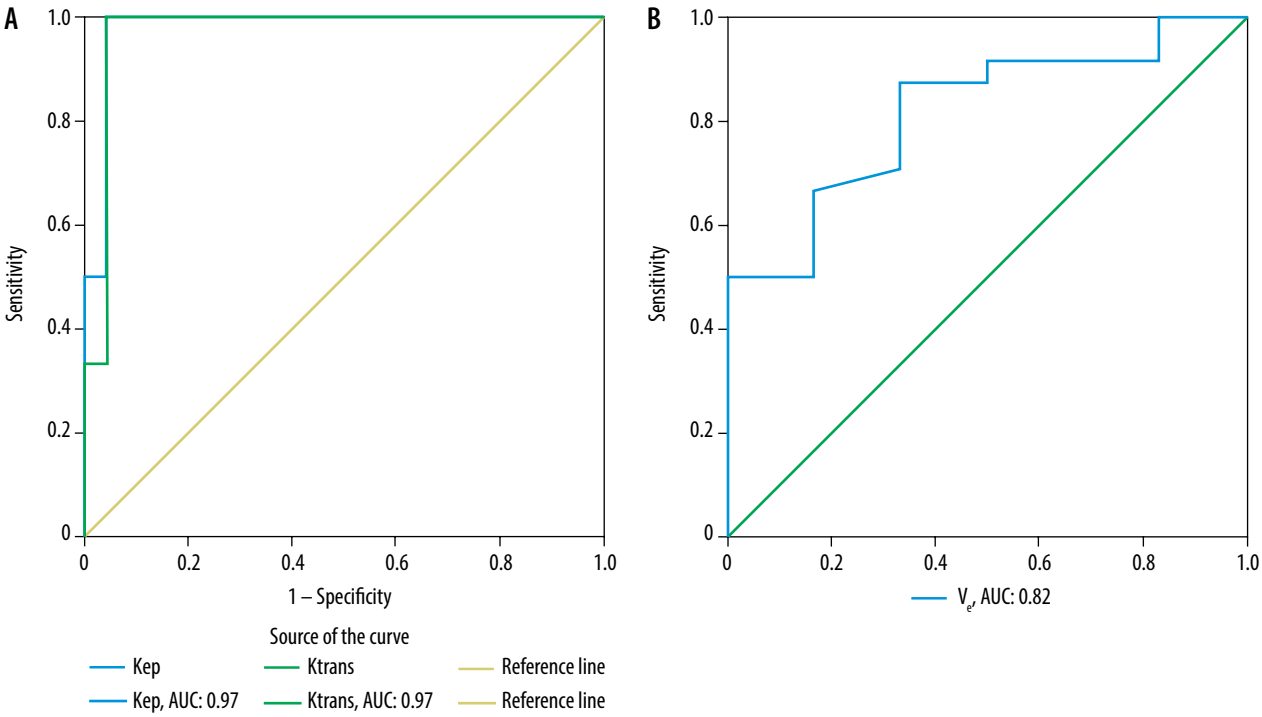

Figure 7. ROC curve analysis of quantitative DCE-MRI parameters (Kep, Ktrans, and Ve) for the prediction of Warthin tumours

Normalized ADC values stabilized the ADC values, which are often affected by different individual physiological characteristics; for example, basal metabolic rate and respiratory rate [7]. Mean normalized ADC was found to be significant in differentiating pleomorphic adenomas, Warthin tumours and malignant tumours ($p < 0.001$). A cut-off 78% and –88% was determined to predict pleomorphic adenomas and Warthin tumours, respectively.

HI indicates heterogeneity of ADC in the lesion. The greater the HI of a lesion, the more heterogenous its ADC. Like other DWI parameters, significant differences were found between the HI of pleomorphic adenomas, Warthin tumours and malignant tumours ($p \leq 0.001$). HI was the highest for Warthin tumours and lowest for pleomorphic adenomas. Sun *et al.* [8] compared the HI of pleomorphic adenomas, Warthin tumours and normal

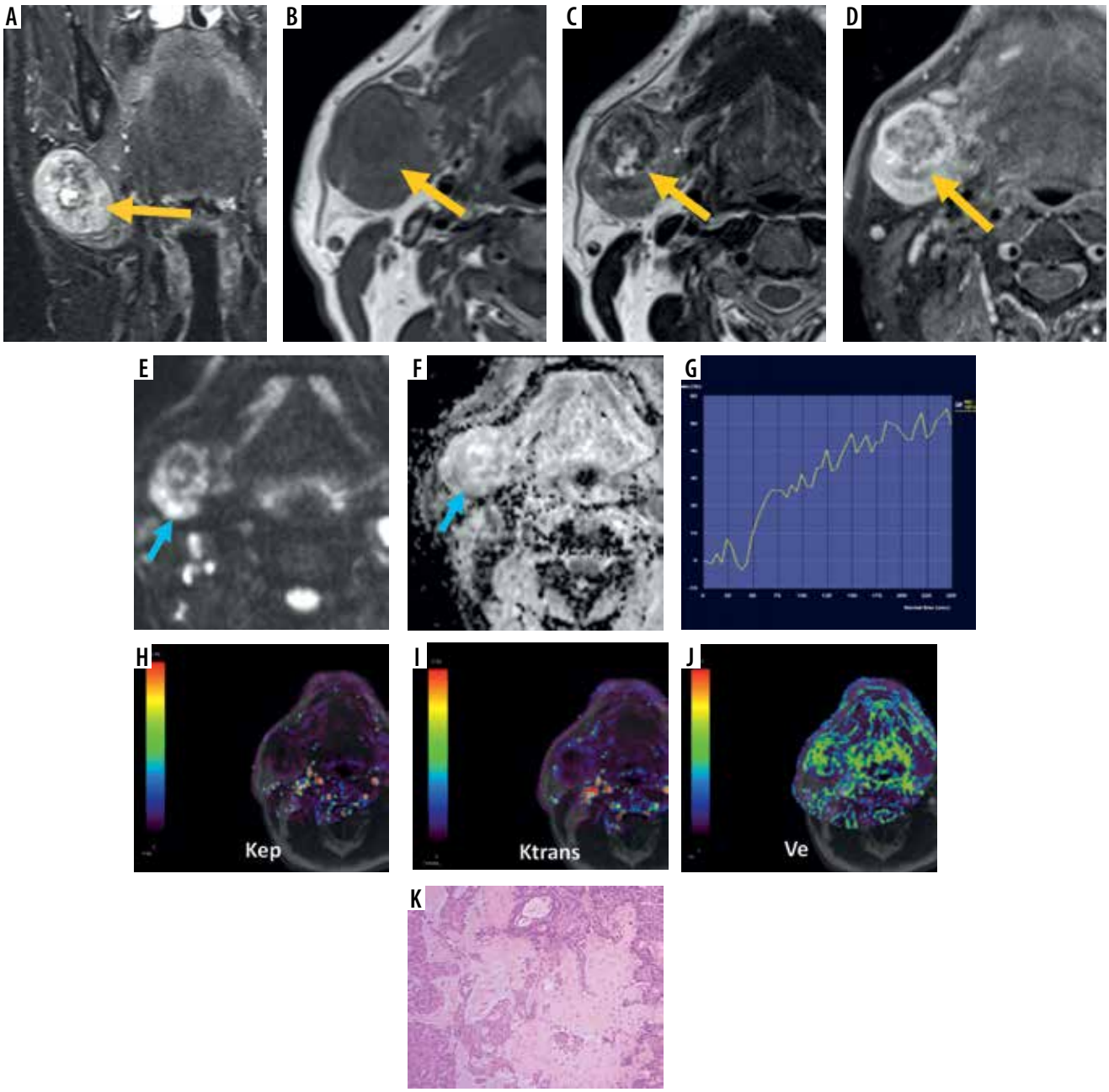

Figure 8. A 50-year-old male with pleomorphic adenoma of the submandibular gland. STIR coronal **(A)**, T1W (**B**), T2W **(C)**, and post-contrast T1-fat saturated (**D**) axial images reveal a relatively well-defined lesion in right submandibular gland appearing isointense on T1W image, heterogeneously iso- to hypointense with few hyperintense areas on T2W image, hyperintense on STIR image, and shows heterogeneous post-contrast enhancement (yellow solid arrows). On DW image **(E)** and corresponding ADC image **(F)**, the lesion shows foci of mild restricted diffusion (blue solid arrows) with mean ADC of 1.18×10^{-3} mm^2/s. On DCE-MRI, the lesion shows type A TIC pattern **(G)** and perfusion colour maps (**H**, **I** and **J**) revealing low K_{ep} (0.029 min^{-1}) and K_{trans} (0.029 min^{-1}) and high V_e (0.999). Dynamic imaging favours the diagnosis of pleomorphic adenoma while morphological and diffusion imaging is atypical. Histopathological image (haematoxylin & eosin 400×) **(K)** shows islands of hyaline cartilage with epithelial cells in small groups, tubules, and glandular architecture

parotid parenchyma with 12 different ROIs and found that the HI of pleomorphic adenomas was significantly lower than that of Warthin tumours.

Dynamic contrast-enhanced MRI

Type A TIC curve was found to be significant in diagnosing pleomorphic adenomas, type B curve was significant in diagnosing Warthin tumours and type C could predict malignancy with high sensitivity, specificity and accuracy (Figure 3, Tables 5 and 6).

Time to peak (TTP) and washout ratio (WR) obtained from the TIC correlated with microvessel count (reflecting tumours vascularity) and stromal cellularity grade, respectively [9]. Type A TIC (slow progressive enhancement) with a late TTP and lack of washout in pleomorphic adenoma reflects its poor vascularity and less cellular stroma with gradual accumulation of contrast in the large

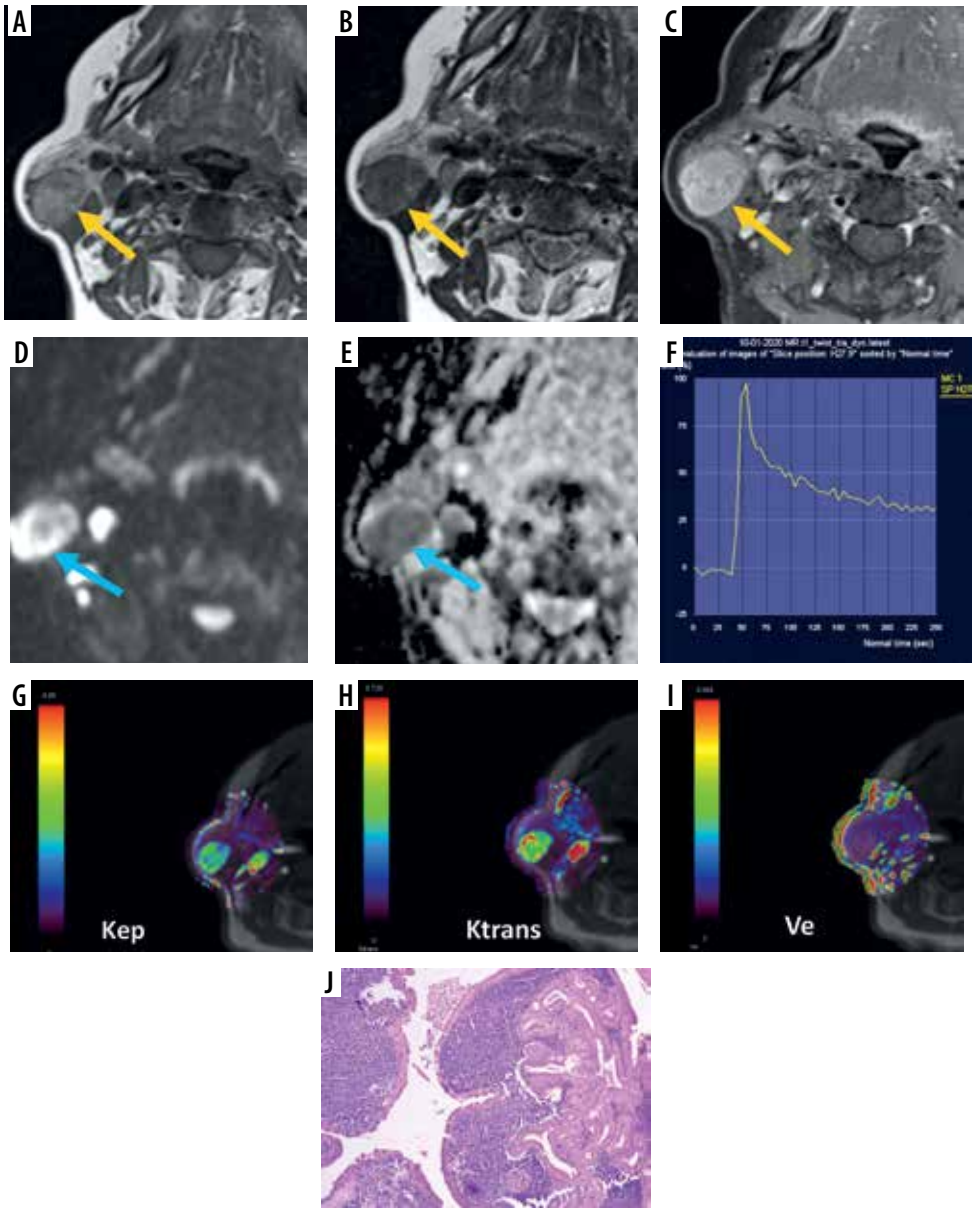

Figure 9. A 76-year-old female with Warthin tumour. T1W **(A)**, T2W **(B)**, and post-contrast T1 fat-saturated **(C)** axial images reveal a well-defined, oval shaped T1 hyperintense (relative to muscles) and T2 hypointense (relative to normal parotid gland) solid mass lesion in the superficial lobe of the right parotid gland with homogeneous post-contrast enhancement (yellow solid arrows). On DW image **(D)** and corresponding ADC image **(E)**, the lesion shows restricted diffusion (blue solid arrows) with a mean ADC of 0.65×10^{-3} mm^2/s. DCE MRI shows type B TIC pattern **(F)** and perfusion colour maps **(G, H** and **I)** revealing high K_{ep} (4.466 min^{-1}) and K_{trans} (0.477 min^{-1}) and low V_e (0.107). Diffusion and dynamic imaging favour the diagnosis of Warthin tumours. Histopathological image (haematoxylin & eosin 400×) **(J)** shows cystic areas with papillary projections lined by oncocytic cells in glandular architecture with dense lymphoid stroma

extracellular (myxoid and chondroid) matrix (Figure 8). On the other hand, early enhancement with early TTP and high washout (type B curve) in Warthin tumours reflects high vascularity and high stromal cellularity of these tumours (Figure 9). Type C TIC in malignant salivary gland tumours reflects high vascularity due to neo-angiogenesis but low stromal cellularity [9] (Figure 10).

Quantitative DCE perfusion MRI provides useful physiological information about capillary permeability, vascular space and extravascular extracellular space (EES). Due to neovascularization in tumours, contrast agent can pass through these newly formed leaky blood vessels into the EES and vice-versa. K_{trans} represents the volume transfer constant from blood plasma to EES, K_{ep} represents the rate constant from EES to plasma and V_e represents the EES fractional volume.

The quantitative DCE parameters were significant in differentiating pleomorphic adenomas, Warthin tumours and malignant tumours from each other. While K_{trans} provides information about perfusion and permeability of the tumour, K_{ep} values corresponds to the washout ratio, which in turns reflects stromal cellularity [12,21]. Pleomorphic adenomas showed the lowest mean K_{ep} and K_{trans} and the highest mean V_e among the 3 groups and Warthin tumours had the highest mean K_{ep} and K_{trans} val-

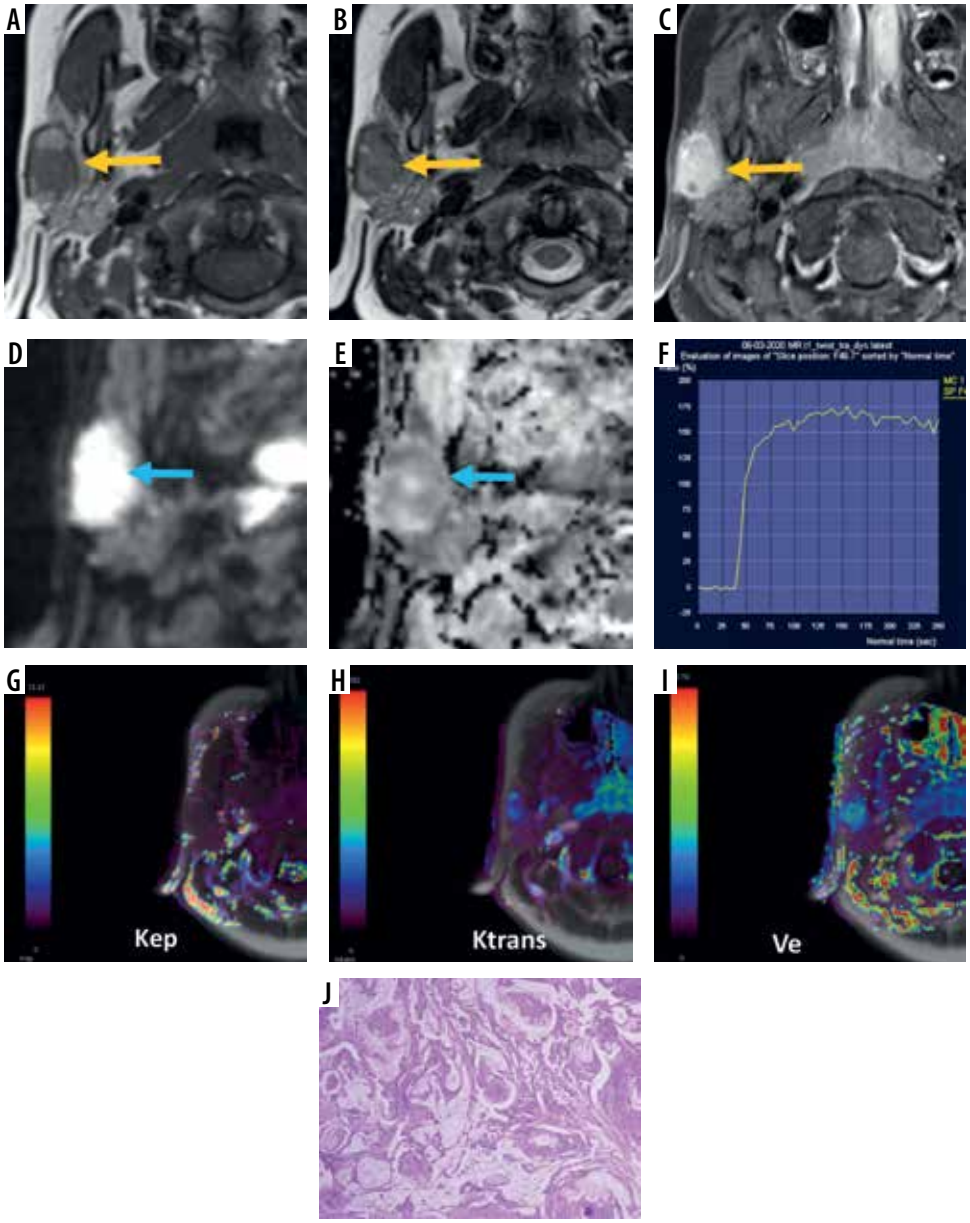

Figure 10. A 12-year-old male with mucoepidermoid carcinoma. T1W **(A)**, T2W **(B)**, and T1 fat-saturated **(C)** axial images reveal a relatively well-defined lesion in the superficial lobe of the right parotid gland, appearing heterogeneously isointense on both T1W (relative to muscles) and T2W (relative to normal parotid gland) images with heterogeneous post-contrast enhancement (yellow solid arrows). DW image **(D)** and corresponding ADC image **(E)** reveals mild restricted diffusion (blue solid arrows) with mean ADC: 1.12×10^{-3} mm^2/s. On DCE MRI, the lesion shows type C TIC pattern **(F)** and perfusion colour maps (**G, H** and **I**) revealing intermediate K_{ep} (0. 681 min^{-1}) and K_{trans} (0.227 min^{-1}), suggesting a malignant lesion. However, V_e of the lesion was slightly higher (0.333). Histopathological image (haematoxylin & eosin 400×) **(J)** shows solid and cystic areas with mucin secreting tumour cells, pools of mucin, and transitional cells

ues and the lowest V_e. Cut-offs were determined using ROC curves in diagnosing pleomorphic adenomas and Warthin tumours, as shown in Tables 5 and 6, respectively. Lower K_{trans} and lower K_{ep} in pleomorphic adenoma indicates lower blood flow through the tumour and lack of washout, respectively, whereas higher V_e indicates its large EES (containing abundant myxoid and chondroid matrices). Conversely, high K_{trans}, high K_{ep} and low V_e for Warthin tumours is most likely related to their higher vascularity, high WR and limited EES because these are highly cellular tumours. Xu *et al.* [22] also determined the diagnostic efficiency of these quantitative DCE parameters in differentiating various salivary gland tumours; however, they did not provide any cut-off values for the same.

There were some limitations in the study. The major limitation was the small sample size. A larger study population with more lesions of each type would have enabled a more comprehensive evaluation. Secondly, histopathological confirmation of diagnosis could only be obtained in 26 patients. In 6 cases of Warthin tumours the diagnosis was formed on the basis of cytological findings alone because these patients opted out of surgical management. Another limitation was different area of ROI in different

tumours due to the variable solid enhancing component, which might have influenced quantitative measurements.

Conclusions

DCE MRI is the only functional MR technique that aided in differentiation of benign and malignant tumour groups. However, when separated into 3 prototype groups of pleomorphic adenomas, Warthin tumours and malignant tumours, each group with different prognosis and management, both DWI and DCE aided in differentiation. However, DCE parameters had higher accuracy in the differentiation of various tumour subgroups than diffusion imaging with comparable accuracy of both semiquantitative TIC pattern and quantitative DCE parameters. Hence, clinical evaluation of salivary gland tumours may be done with the addition of semiquantitative dynamic contrast-enhanced imaging to standard morphological imaging, which contributes immense value to the study, with a time penalty of only about 4 minutes and a short learning curve.

Conflict of interest

The authors report no conflict of interest.

References

1. Christe A, Waldherr C, Hallett R, et al. MR imaging of parotid tumors: typical lesion characteristics in MR imaging improve discrimination between benign and malignant disease. AJNR Am J Neuroradiol 2011; 32: 1202-1207.
2. Mihashi H, Kawahara A, Kage M, et al. Comparison of preoperative fine-needle aspiration cytology diagnosis and histopathological diagnosis of salivary gland tumors. Kurume Med J 2006; 53: 23-27.
3. Ashraf A, Shaikh AS, Kamal F, et al. Diagnostic reliability of FNAC for salivary gland swellings: a comparative study. Diagn Cytopathol 2010; 38: 499-504.
4. Mallon DH, Kostalas M, MacPherson FJ, et al. The diagnostic value of fine needle aspiration in parotid lumps. Ann R Coll Surg Engl 2013; 95: 258-262.
5. Perkins C, Toll E, Reece P. Fine-needle aspiration cytology and radiological imaging in parotid gland tumours: our experience in 103 patients. Clin Otolaryngol 2019; 44: 1124-1127.
6. Lee YY, Wong KT, King AD, et al. Imaging of salivary gland tumours. Eur J Radiol 2008; 66: 419-436.
7. Zhang W, Zuo Z, Huang X, et al. Value of diffusion-weighted imaging combined with susceptibility-weighted imaging in differentiating benign from malignant parotid gland lesions. Med Sci Monit 2018; 24: 4610-4616.
8. Sun Q, Ma C, Dong M, et al. Effects of region of interest sizes on apparent diffusion coefficient measurements of pleomorphic adenoma, Warthin tumor, and normal parotid parenchyma. Quant Imaging Med Surg 2019; 9: 681-690.
9. Yabuuchi H, Fukuya T, Tajima T, et al. Salivary gland tumors: diagnostic value of gadolinium-enhanced dynamic MR imaging with histopathologic correlation. Radiology 2003; 226: 345-354.
10. Eissa L, Abou Seif S, El Desooky S, et al. Accuracy assessment of combined diffusion weighed and dynamic gadolinium MR sequences in characterization of salivary gland tumors. Egypt J Radiol Nucl Med 2016; 47: 127-139.
11. El-Atta M, Amer T, Gaballa G, et al. Multi-phasic CT versus dynamic contrast enhanced MRI in characterization of parotid gland tumors. Egypt J Radiol Nucl Med 2016; 47: 1361-1372.
12. Yabuuchi H, Kamitani T, Sagiyama K, et al. Characterization of parotid gland tumors: added value of permeability MR imaging to DWI and DCE-MRI. Eur Radiol 2020; 30: 6402-6412.
13. Motoori K, Yamamoto S, Ueda T, et al. Inter- and intratumoral variability in magnetic resonance imaging of pleomorphic adenoma: an attempt to interpret the variable magnetic resonance findings. J Comput Assist Tomogr 2004; 28: 233-246.
14. Matsushima N, Maeda M, Takamura M, et al. Apparent diffusion coefficients of benign and malignant salivary gland tumors. Comparison to histopathological findings. J Neuroradiol 2007; 34: 183-189.
15. Habermann CR, Arndt C, Graessner J, et al. Diffusion-weighted echo-planar MR imaging of primary parotid gland tumors: is a prediction of different histologic subtypes possible? AJNR Am J Neuroradiol 2009; 30: 591-596.
16. Zheng N, Li R, Liu W, et al. The diagnostic value of combining conventional, diffusion-weighted imaging and dynamic contrast-enhanced MRI for salivary gland tumors. Br J Radiol 2018; 91: 20170707. doi: 10.1259/bjr.20170707.
17. Xu Z, Chen M, Zheng S, et al. Differential diagnosis of parotid gland tumours: application of SWI combined with DWI and DCE-MRI. Eur J Radiol 2022; 146: 110094. doi: 10.1016/j.ejrad.2021.110094.
18. Karaman Y, Özgür A, Apaydın D, et al. Role of diffusion-weighted magnetic resonance imaging in the differentiation of parotid gland tumors. Oral Radiol 2016; 32: 22-32.
19. Karaman CZ, Tanyeri A, Özgür R, et al. Parotid gland tumors: comparison of conventional and diffusion-weighted MRI findings with histopathological results. Dentomaxillofac Radiol 2021; 50: 20200391. doi: 10.1259/dmfr.20200391.
20. Yabuuchi H, Matsuo Y, Kamitani T, et al. Parotid gland tumors: can addition of diffusion-weighted MR imaging to dynamic contrast-enhanced MR imaging improve diagnostic accuracy in characterization? Radiology 2008; 249: 909-916.
21. Gaddikeri S, Gaddikeri RS, Tailor T, et al. Dynamic contrast-enhanced MR imaging in head and neck cancer: techniques and clinical applications. AJNR Am J Neuroradiol 2016; 37: 588-595.
22. Xu Z, Zheng S, Pan A, et al. A multiparametric analysis based on DCE-MRI to improve the accuracy of parotid tumor discrimination. Eur J Nucl Med Mol Imaging 2019; 46: 2228-2234.